

ARTICLE

## Evaluation of the Mechanisms Acting on the Atlantic Meridional Overturning Circulation in CESM2 for the 1pctCO<sub>2</sub> Experiment

Lívia Sancho<sup>1\*</sup>, Elisa Passos<sup>2,3</sup>, Marcio Cataldi<sup>4,5\*</sup>, Luiz Paulo de Freitas Assad<sup>1,6</sup>, Luiz Landau<sup>1</sup>

<sup>1</sup> Laboratory of Computational Methods in Engineering, Civil Engineering Program, Alberto Luiz Coimbra Institute for Graduate Studies and Research in Engineering, Federal University of Rio de Janeiro, Rio de Janeiro, 21941-617, Brazil

<sup>2</sup> Civil Engineering Program, Alberto Luiz Coimbra Institute for Graduate Studies and Engineering Research, Federal University of Rio de Janeiro, Rio de Janeiro, 21941-617, Brazil

<sup>3</sup> Physical Oceanography Laboratory, Department of Physical Oceanography, Faculty of Oceanography, Rio de Janeiro State University, Rio de Janeiro, 20559-900, Brazil

<sup>4</sup> Climate System Monitoring and Modeling Laboratory, Water Resources and Environmental Engineering, Fluminense Federal University, 24020-140, Brazil

<sup>5</sup> Regional Atmospheric Modeling Group (MAR), Physics of the Earth, Department of Physics, Regional Campus of International Excellence (CEIR) "Campus Mare Nostrum", University of Murcia, Murcia, 30100, Spain

<sup>6</sup> Department of Meteorology, Institute of Geosciences, Federal University of Rio de Janeiro, Rio de Janeiro, 21941-617, Brazil

### ABSTRACT

The Atlantic Meridional Overturning Circulation (AMOC) is a crucial component of the Earth's climate system due to its fundamental role in heat distribution, carbon and oxygen transport, and the weather. Other climate components, such as the atmosphere and sea ice, influence the AMOC. Evaluating the physical mechanisms of those interactions is paramount to increasing knowledge about AMOC's functioning. In this study, the authors used outputs from the Community Earth System Model version 2 and observational data to investigate changes in the AMOC and the associated physical processes. Two DECK experiments were evaluated: piControl and 1pctCO<sub>2</sub>, with an annual increase of 1% of atmospheric CO<sub>2</sub>. The analysis revealed a significant decrease in the AMOC, associated with changes in mixed layer depth and buoyancy in high latitudes of the North Atlantic, resulting in the shutdown of deep convection and potentially affecting the formation of North Atlantic Deep Water and Antarctic Bottom Water. A vital aspect observed in this study is the association between increased runoff and reduced water evaporation, giving rise to a positive feedback process. Consequently, the rates of freshwater spreading have intensified during this period, which could lead to an accelerated disruption of the AMOC beyond the projections of existing models.

**Keywords:** AMOC; Meridional cell; Climate change; Deep circulation; CESM2 results; CMIP6

#### \*CORRESPONDING AUTHOR:

Lívia Sancho, Laboratory of Computational Methods in Engineering, Civil Engineering Program, Alberto Luiz Coimbra Institute for Graduate Studies and Research in Engineering, Federal University of Rio de Janeiro, Rio de Janeiro, 21941-617, Brazil; Email: liviasancho@coppe.ufrj.br  
Marcio Cataldi, Climate System Monitoring and Modeling Laboratory, Water Resources and Environmental Engineering, Fluminense Federal University, 24020-140, Brazil; Regional Atmospheric Modeling Group (MAR), Physics of the Earth, Department of Physics, Regional Campus of International Excellence (CEIR) "Campus Mare Nostrum", University of Murcia, Murcia, 30100, Spain; Email: marcioataldi@um.es

#### ARTICLE INFO

Received: 6 November 2023 | Revised: 3 January 2024 | Accepted: 10 January 2024 | Published Online: 18 January 2024

DOI: <https://doi.org/10.30564/jasr.v7i1.6070>

#### CITATION

Sancho, L., Passos, E., Cataldi, M., et al., 2024. Evaluation of the Mechanisms Acting on the Atlantic Meridional Overturning Circulation in CESM2 for the 1pctCO<sub>2</sub> Experiment. Journal of Atmospheric Science Research. 7(1): 40–58. DOI: <https://doi.org/10.30564/jasr.v7i1.6070>

#### COPYRIGHT

Copyright © 2024 by the author(s). Published by Bilingual Publishing Group. This is an open access article under the Creative Commons Attribution-NonCommercial 4.0 International (CC BY-NC 4.0) License (<https://creativecommons.org/licenses/by-nc/4.0/>).

## 1. Introduction

The Industrial Revolution of the 18th and 19th centuries led to a substantial increase in greenhouse gas (GHG) emissions, causing global climate change and rising temperatures<sup>[1,2]</sup>. These changes pose significant concerns for the scientific community, like the increase in frequency and intensity of weather extremes<sup>[3,4]</sup>. Central to the climate system is the Atlantic Meridional Overturning Circulation (AMOC), a complex system responsible for a net northward flow of warm water in the upper layers and a net southward flow of the North Atlantic Deep Water (NADW)<sup>[5-7]</sup>, which is critical for the global climate system. It is responsible for alleviating the harsh winters in Europe, along with the westerlies of that region<sup>[8-10]</sup>. Furthermore, the AMOC plays a vital role in the uptake and distribution of essential tracers such as heat, carbon, and oxygen<sup>[8]</sup>.

Recent models highlight a strong link between deepwater formation at high latitudes in the North Atlantic Ocean and the AMOC's intensity<sup>[11]</sup>. The AMOC's sensitivity to evaporation is limited unless the flow is reduced to values close to 0.03 Sv, and a freshwater build-up of 0.32 Sv in the Atlantic can lead to lower local density and shut off the deep convection<sup>[12]</sup>. Other studies estimate a freshwater build-up between 0.1 and 0.5 Sv, highlighting the critical role of freshwater input in modulating the AMOC strength and the potential for even small changes in this term to significantly impact the global climate system<sup>[13]</sup>. Freshwater input can result in changes to the northward heat transport and heat release in the North Atlantic region, with impacts beyond the Atlantic Ocean<sup>[14]</sup>. Therefore, understanding the AMOC is crucial for researchers and government decision-making<sup>[15,16]</sup>. The studies<sup>[17,18]</sup> demonstrated the potential for freshwater input to impact the AMOC and global climate system significantly.

This study aims to investigate the impact of increasing atmospheric concentrations of CO<sub>2</sub> on the AMOC and associated ocean, sea ice, and atmosphere interactions. Thus, a high-emission CO<sub>2</sub> experiment from the Community Earth System Model version 2, combined with observational data, was used.

Our analysis seeks to identify changes in the AMOC and estimate different terms to gain insight into the evolution of the AMOC in the current climate and assess how close we are to crossing a critical climate breaking point.

The paper is structured as follows: In Section 2, we describe the data sources, the Earth System model, and experimental setup, as well as the methodology for implemented analysis. Section 3 presents and discusses our findings, focusing on RAPID data and Meridional Overturning, the mixed layer depth, and the freshwater input to the North Atlantic Ocean. Finally, we summarize our conclusions and offer some final remarks in Section 4.

## 2. Methodology

We used observational data and Earth System modeling results to evaluate the effects of atmospheric CO<sub>2</sub> on AMOC behavior. The following sections will describe the model outputs, the observational data, and the mathematical framework. This methodology provides a comprehensive approach to evaluate the impact of increasing atmospheric CO<sub>2</sub> on AMOC and related processes, which is essential for predicting the future of our climate and its potential impacts on global ecosystems.

### 2.1 Model description

This article analyzes the behavior of the AMOC patterns under a climate change scenario using the results of the state-of-the-art Earth System model Community Earth System Model version 2 (CESM2)<sup>[19]</sup>. CESM2 is the latest version of the National Center for Atmospheric Research (NCAR) Earth System model and the one used to perform simulations of the Coupled Model Intercomparison Project Phase 6 (CMIP6)<sup>[20]</sup>. Its design aims to simulate the physical, chemical, and human components that govern the climate system and the intrinsic feedback system on timescales of hundreds of years or more.

The CESM2 experiments used five components to represent various elements of the Earth system (atmosphere, ocean, land surface, sea ice, and river

runoff) in a nominal  $1^\circ$  horizontal resolution<sup>[20]</sup>. The various components of the Earth System and their interactions are modeled as follows: The Community Atmosphere Model version 6.0 (CAM6)<sup>[21]</sup> is used for the atmospheric component. This version includes aerosol-activated cloud droplet formation, and it models precipitation processes due to the size of condensation nuclei and the interaction between cloud particles in an explicit way.

The Community Land Model version 5 (CLM5)<sup>[22,23]</sup> is used for the land component. It quantifies the physical, chemical, and biological processes by which terrestrial ecosystems affect and are affected by climate across various spatial and temporal scales. The model consists of multiple components related to biogeophysics, hydrologic cycle, biogeochemistry, and ecosystem dynamics<sup>[24]</sup>.

The Community Ice Code version 4 (CICE)<sup>[25]</sup> simulates the sea-ice interaction. It calculates local snow and ice growth rates due to radiative, conductive, and turbulent fluxes and ice dynamics<sup>[26,27]</sup>, includes multiple scattering shortwave radiation treatment<sup>[28]</sup>, and explicitly simulates the evolution of melt pools of ice (melt pond) and the deposition and cycling of dust aerosols and black carbon in the ice sheet<sup>[29]</sup>. The ice thickness distribution follows<sup>[30]</sup>.

The Model for Scale Adaptive River Transport (MOSART)<sup>[31]</sup> accounts for river transport with the primary objective of providing freshwater input data to the ocean model. Surface runoff is routed across slopes and discharged along with subsurface runoff into a sub-grid before entering the main channel. Channel velocities and water depth in the channel varying in time are considered. River flow is determined by a kinematic wave method.

Although the results of the experiments were simulated using all five components, the oceanic outputs—ocean fields and fluxes from other components—were the focus of this study. The ocean component of CESM is version 2 of the Parallel Ocean Program model (POP2), developed by Los Alamos National Laboratory (LANL)<sup>[32]</sup>. POP2 is a general global ocean circulation model that solves primitive ocean dynamics equations in three dimensions using the

hydrostatic and Boussinesq approximations<sup>[24,32]</sup>. The model is vertically discretized in z-coordinates<sup>[32,33]</sup> with 60 vertical levels. The ocean has a thickness of 10 m from the surface to 160 m. Below that depth, the thickness gradually increases to 250 m at 3500 m, which remains constant until the bottom (5500 m)<sup>[20]</sup>.

## 2.2 Experimental setup

Results from two scientifically validated CMIP6 experiments were used to evaluate how the AMOC reacts to a greenhouse's worsening climate<sup>[20,34]</sup>. They are part of the CMIP6 Diagnostic, Evaluation, and Characterization of Klima (DECK) experiments. The piControl experiment represents the preindustrial period with non-evolving conditions, while the 1pctCO<sub>2</sub> experiment simulates an exponential annual 1% increase in atmospheric CO<sub>2</sub> concentration. GHG concentrations<sup>[35]</sup> were used for both experiments. The DECK experiments are crucial for understanding how the Earth's climate will respond to increasing greenhouse gas concentrations, and they have been used extensively in previous climate research<sup>[34]</sup>. Interested readers can find more technical details about these experiments in various sources<sup>[20,36–39]</sup> and others.

### *piControl experiment*

The piControl experiment was designed to simulate the preindustrial period with non-evolving conditions, using 1850 as a reference year. This experiment aims to evaluate the coupled system and study the unforced variability of the climate system, serving as a baseline for other experiments that branch from it<sup>[34]</sup>. The assumptions made for the piControl are the following. There are no secular changes in forcing (concentrations of atmospheric constituents and land use are fixed), and the Earth's orbital characteristics are constant. That way, since there are no changes in forcing, natural or anthropogenic, the piControl is suited to study the internal variability of the climate system<sup>[34]</sup>.

piControl simulation started after a spin-up for the model to come into balance with the forcing, and it was run for 1200 years, but we only used the first 500 years of it. The top-of-the-atmosphere global-

and time-mean heat fluxes were controlled through tuning, resulting in an average imbalance of  $+0.05 \text{ W}\cdot\text{m}^{-2}$  [20]. These adjustments remained fixed for the subsequent simulations from this experiment, such as the 1pctCO<sub>2</sub> experiment. The climatological state of piControl was validated by comparing it with observations, reanalysis, and descriptions in the literature, making it suitable for reference for the 1pctCO<sub>2</sub> experiment. Although piControl's validation is a necessary process, it is beyond the scope of this paper to discuss its results.

### **1pctCO<sub>2</sub> experiment**

The 1pctCO<sub>2</sub> is an idealized climate change experiment designed to simulate the climate system's response to a gradual increase in atmospheric CO<sub>2</sub> concentrations [40]. This experiment was branched from year 501 of piControl and involves a yearly rise in 1% of atmospheric CO<sub>2</sub> concentration from the annual global mean value of 1850 (284.3 ppm) [34,35,40]. To ensure that the 1pctCO<sub>2</sub> is reliable, the simulation is run for at least 150 years beyond the quadrupling of CO<sub>2</sub> at year 140 [34].

To compare 1pctCO<sub>2</sub> experiment results to observations, we used Mauna Loa CO<sub>2</sub> emissions values during the RAPID 15-year period (382.09–414.24 ppm) and identified a similar emission period in the 1pctCO<sub>2</sub> experiment. Since 1pctCO<sub>2</sub> is an idealized experiment, CO<sub>2</sub> intervals between both products serve to evaluate the model performance. That way, the 1pctCO<sub>2</sub> experiment period was divided into three different periods. The period with an emissions interval similar to RAPID was called R-1pctCO<sub>2</sub> (model years 32–40) to represent the current climate. The remaining 1pctCO<sub>2</sub> period after R-1pctCO<sub>2</sub> is called F-1pctCO<sub>2</sub> (model years 41–150) and represents the future state of the climate. To facilitate analysis, we also defined L-1pctCO<sub>2</sub> (model years 141–150) as the last decade of the 1pctCO<sub>2</sub> experiment. The article uses piControl as a synonym for the past climate.

## **2.3 Observational data**

### **RAPID data for the AMOC estimation**

We evaluated the present AMOC using data from

the Rapid Climate Change Meridian Overturning Circulation and Heatflux array (RAPID array) [41]. We then compared the results with the model outputs to validate them using CO<sub>2</sub> measurements from Mauna Loa. The RAPID array consists of a series of moorings along the 26.5°N parallel, spanning from Morocco to Florida, measuring temperature, salinity, and velocity of currents from near the surface to the bottom [42]. The goal of this array is to continuously monitor the strength and structure of the AMOC [43]. Further details on the RAPID moorings can be found [43,44].

We used horizontally integrated and monthly profiles from the RAPID array from 2005 to 2019. The RAPID profiles cover the surface until almost 6000 m, with an average vertical resolution of 19.59 m (19.33–19.87 m). We extracted time series as the maximum profile value at each time, and vertical equivalence to match and compare RAPID to the model output's vertical resolution was achieved through nearest-neighbor interpolation, degrading RAPID's vertical resolution.

### **Mauna Loa CO<sub>2</sub> measuring**

The Mauna Loa Observatory in Hawaii (19.5°N, 155.6°W) has collected CO<sub>2</sub> measurements since 1958, making it the oldest site for such data [2]. CO<sub>2</sub> records were obtained from the National Oceanic and Atmospheric Administration (NOAA) website, the organization responsible for acquiring these data. The monthly measurements from November 1962 to October 2021 were used to estimate CO<sub>2</sub> emissions during the RAPID period and find a similar emission period in the model outputs.

## **2.4 Mathematical framework**

The AMOC is a variable provided by POP2 as the Eulerian mean of the total transport for the Atlantic Ocean, Mediterranean Sea, Labrador Sea, GIN Sea, Arctic Ocean, and Hudson Bay. It is provided as a variable dependent on depth, latitude, and time. It was used to evaluate the meridional overturning at 26.5°N. The North Atlantic Ocean's total surface freshwater flux (FW) was calculated using Equations (1) and (2) to assess the region's freshwater changes. The green-shaded area in **Figure 1** shows the region

of interest for this analysis, which has also been used in previous studies <sup>[17,45,46]</sup>. Understanding freshwater inputs to the North Atlantic Ocean is important because they can impact ocean circulation and climate patterns.

$$FW = \frac{(P-E+R+M_{ice}+Salt+F_{ice}) \cdot ocean\_area}{\rho} \quad (1)$$

$$F_{ice} = Q/L_f \quad (2)$$

where:

- i.  $P$  is the precipitation flux (rain + snow) in  $kg \cdot m^{-2} \cdot s^{-1}$ .
- ii.  $E$  is the evaporation flux in  $kg \cdot m^{-2} \cdot s^{-1}$ .
- iii.  $R$  is the river runoff flux (liquid + frozen) in  $kg \cdot m^{-2} \cdot s^{-1}$ .
- iv.  $M_{ice}$  is the melting of sea ice in  $kg \cdot m^{-2} \cdot s^{-1}$ .
- v.  $Salt$  is the salt flux due to ice melt in  $kg \cdot m^{-2} \cdot s^{-1}$ .
- vi.  $F_{ice}$  is the contribution of frazil ice formation.
- vii.  $ocean\_area$  is the surface area of the ocean in  $m^2$ .
- viii.  $\rho$  is the ocean density in  $kg \cdot m^{-3}$ .
- ix.  $Q$  is the ocean heat flux due to ice formation in  $W \cdot m^{-2}$ .
- x.  $L_f$  is the latent heat of fusion in  $J \cdot kg^{-1}$  ( $W = J \cdot s^{-1}$ ).

To estimate buoyancy in the North Atlantic Ocean, we adopted the methodology <sup>[47]</sup> and applied Equation (3) to the red polygons depicted in **Figure 1**. These regions were selected based on the significant shallowing of the mixed layer depth in March, as discussed in the results section. Buoyancy is a critical term for comprehending ocean circulation and climate dynamics since it provides insight into the vertical stratification of the ocean.

$$B = \frac{g\alpha(Q_s - L_v E)}{c_p} - g\beta(E - P)S + gR \quad (3)$$

where:

- i.  $g$  is the acceleration due to gravity of  $9.81 \text{ ms}^{-2}$ .
- ii.  $\alpha$  is the thermal expansion coefficient in  $K^{-1}$  ( $-\rho^{-1} \partial \rho / \partial T$ ).

iii.  $Q_s$  is the heat flux due to radiation and conduction processes at the ocean-atmosphere interface in  $W \cdot m^{-2}$ .

iv.  $L_v$  is the latent heat of evaporation of  $25.01 \cdot 10^5 \text{ J} \cdot kg^{-1}$ .

v.  $c_p$  is the specific heat at constant pressure in  $J \cdot kg^{-1} \cdot K^{-1}$ .

vi.  $\beta$  is the saline contraction coefficient ( $-\rho^{-1} \partial \rho / \partial S$ ).

vii.  $S$  is the salinity.

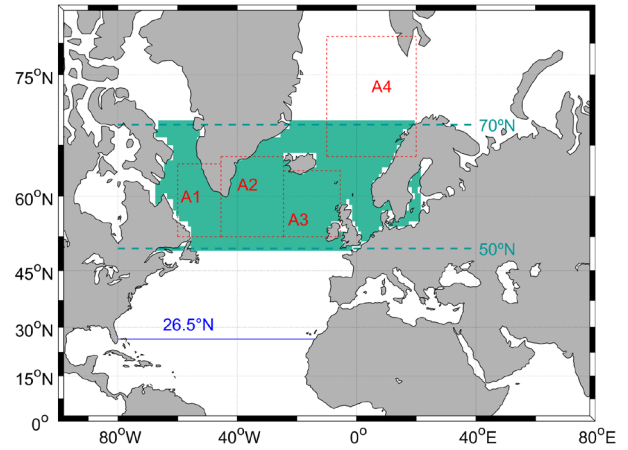


**Figure 1.** Regions evaluated in this work. The red polygons are areas where the depth of the mixed layer and the buoyancy associated with the vertical stratification of the ocean were analyzed. The green region assesses freshwater flux into the North Atlantic Ocean. The blue line is the section where the meridional overturning was evaluated.

**Figure 1** was also used to assess the depth profile and time series of the meridional transport in the model results and RAPID using the blue transect and to estimate the mixed layer depth in the regions marked by the red polygons. The geographic boundaries of the areas in **Figure 1** are presented in **Table 1**. The mixed-layer depth is a crucial term that affects the exchange of heat and salt between the atmosphere and the ocean. The POP2 code uses the method <sup>[48]</sup> to estimate the mixed-layer depth. This method considers the effects of turbulent mixing on the vertical distribution of buoyancy and provides a reliable estimate of the mixed-layer depth.

We employed the Decision Tree method to analyze the importance of different forcing mechanisms on the freshwater flux to the North Atlantic throughout the

experiments<sup>[49–51]</sup>. This method is a nonlinear model that splits the data into a series of decision nodes, each representing a critical point for simulating the resultant freshwater flux. We used the average time series of freshwater flux in the green region of **Figure 1** as the dependent variable and the main terms, including frazil ice formation, evaporation flux, sea ice melting flux, precipitation flux, and river runoff flux, as the independent variables. The Decision Tree algorithm calculates the importance of each independent variable in conceiving the dependent one and provides statistical quantities, such as RMSE and  $R^2$ , to evaluate its accuracy<sup>[51]</sup>.

**Table 1.** Geographic limits of the regions used in the analysis of **Figure 1**.

Region	Latitude	Longitude
Area 1	52.5°N–65°N	60°W–45.5°W
Area 2	52.5°N–66°N	45.5°W–24.5°W
Area 3	52.5°N–64°N	24.5°W–5.5°W
Area 4	66°N–78°N	10°W–20°E
26.5°N	26.5°N	80°W–14°W

Decision Tree Regressor is a powerful technique for environmental data since it can handle large amounts of values and a smaller number of variables<sup>[52]</sup>. The Decision Tree was implemented as a training set for the 500y of piControl, the 150y of 1pctCO<sub>2</sub>, the 9y of R-1pctCO<sub>2</sub>, the 110y of the F-1pctCO<sub>2</sub> and the 10y of L-1pctCO<sub>2</sub>, with monthly frequency, to evaluate changes in the predictors of freshwater flux with six nodes.

Throughout the article, we used statistical quantities to analyze the relationships between variables. These included mean, median, variance, standard deviation, correlation, and  $R^2$ . All the correlations in this article are significant at the 95% confidence level, and we consider strong correlations above 0.70. The lag was estimated as the time of maximum correlation between both time series. These statistical quantities provide valuable insights into the system's behavior and the interplay between different terms.

## 3. Results and discussion

### 3.1 RAPID data and meridional overturning

**Figure 2** displays the time series of the overturning transport, both integrated on the water column (panel a) and as a depth profile of the RAPID moorings in the 26.5°N parallel (panel b). The integrated overturning transport represents the total volume of water moved by the AMOC per unit time, which is generally positive, with a mean value of 16.91 Sv and a standard deviation of 4.59 Sv. However, we observe dips of approximately 26% in 2009/2010, 17% in 2012/2013, and 12% in 2018/2019, consistent with previous studies<sup>[44,53,54]</sup>. These dips are related to changes in ocean circulation, freshwater input, and atmospheric forcing.

The depth profile (**Figure 2b**) shows northward transport from the surface to deep depths and southward transport below them, reflecting the upper and lower branches of the AMOC cell. The transport inversion exhibits significant variability, with depths ranging from near the surface (59.60 m) to the bottom (5956.40 m) and an average inversion depth of 4230.92 m. At times, we also observe southward transports from near the surface to the bottom, as reflected by the dips in the time series (**Figure 2a**). The variability in the AMOC is primarily driven by high-frequency variability in zonal winds<sup>[53]</sup>, and the RAPID measurements were taken during the warm (positive) phase of the Atlantic Multidecadal Variability.

The R-1pctCO<sub>2</sub> period, corresponding to model years 32 to 40, has been estimated to represent the RAPID dataset. Hence, the 15-year RAPID time series is equivalent to 9 years of an intensive emission experiment through CO<sub>2</sub> measurements, which allows us to observe the current high rate of CO<sub>2</sub> emissions. In the left panel of **Figure 3**, we present the statistics of the RAPID data and the experiments. The average value of the time series decreases from the past to the present and future, indicating a weakening of the AMOC. Although the present period has

an average value similar to RAPID, it has lower variability, possibly due to the model’s non-eddy-permitting horizontal resolution, which fails to resolve mesoscale processes. This observation suggests that the model is more conservative in its representation. CMIP6 model biases in the mean climate have been identified, which can influence AMOC response to climate change <sup>[56]</sup>.

In the future (F-1pctCO<sub>2</sub>), the average flux is projected to decrease significantly, with the average dropping to approximately 10 Sv and a substantial increase in the standard deviation. Given the conservative behavior of the model, the future may be even more alarming than what is modeled. Moreover, on F-1pctCO<sub>2</sub>, the median value is lower than the mean, indicating a time series with lower values and higher extremes. Finally, in the last decade, the AMOC overturning has been extremely low, reaching approximately 6 Sv. The mean and median values are similar, and the variations are reduced, characterizing a low, more uniformly distributed overturning.

To provide a detailed evaluation of the AMOC profile, we examine the meridional transport profile in **Figure 3b**. This figure shows all products’ upper and lower branches of the AMOC. While the profile pattern of the present climate is similar to RAPID, there is a noticeable difference in the depth of the lower branch. Despite this discrepancy, **Figure 3c** displays a scatter plot between both products; the high R<sup>2</sup> value indicates

good agreement between them. This difference is likely related to the time required for the deep ocean to stabilize numerically. Nevertheless, this study examines how the system responds to atmospheric forcing and the propagation of forcing through the ocean surface and does not require a stabilized deep ocean.

F-1pctCO<sub>2</sub> shows a significant reduction in the AMOC upper limb and a shallowing of the lower limb compared to RAPID, with L-1pctCO<sub>2</sub> intensifying this behavior. The upper limb retreats from its maximum value of 22.02 Sv at 928.04 m and 34°N to 13.51 Sv at 60.00 m and 12°N (not shown), resulting in less heat reaching high latitudes in the North Atlantic. This weakening may have responded to changes in the mixed layer depth and the shut-down of deep convection. Moreover, the meridional transport behavior in L-1pctCO<sub>2</sub> can be attributed to a decrease in NADW formation and an increase in AABW formation, possibly caused by changes in the salinity gradient of the sea surface between the Southern Ocean and the North Atlantic Ocean. This freshening is noticeable in the North Atlantic Ocean, as shown in **Figures 4c and 4e**. Strengthening AABW formation and decreasing NADW formation may have caused AABW to spread through the deep Atlantic further north. Additionally, the negative SST trends south of Greenland (**Figures 4d and 4f**), known as the ‘warming hole’, together with strong negative salinity trends in the same region, are consistent with an AMOC slowdown <sup>[57,58]</sup>.

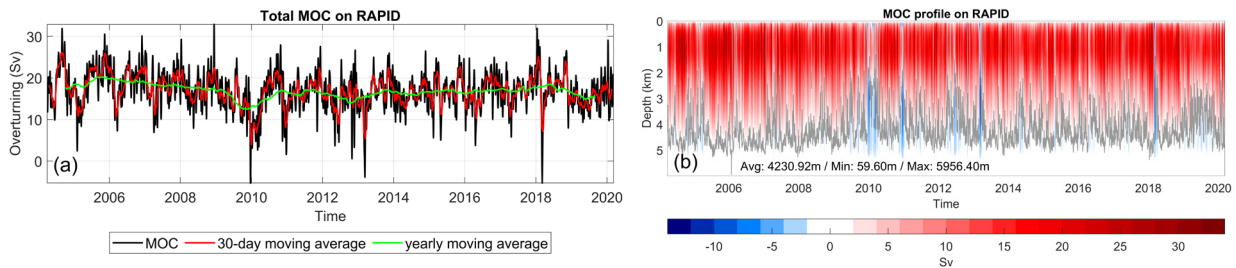


**Figure 2.** Zonally averaged meridional overturning circulation time series estimated by RAPID moorings along the 26.5°N parallel. (a) Vertically integrated, 30-day, and yearly moving average time series, and (b) Profile time series. Positive values (red) are associated with northward transport, and negative values (blue) are associated with southward transport <sup>[55]</sup>. The gray line marks the depth of transport inversion, and the values are the average, minimum, and maximum depths where the inversion occurs.

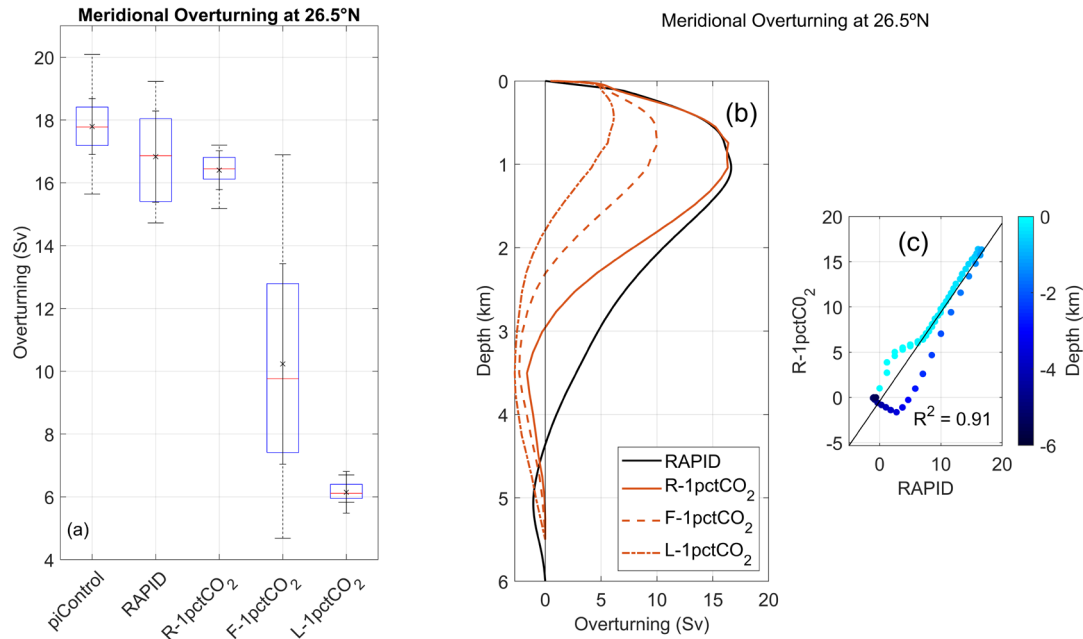


**Figure 3.** Meridional Overturning at 26.5°N. (a) Boxplot showing the distribution of Meridional Overturning (in Sv) across multiple CESM2 experiments and RAPID data. The black x represents the mean of each series, the red line represents the median, and the box corresponds to the data’s 25th and 75th percentiles. The whiskers (solid and dashed) indicate the standard deviation and the range of the data, respectively. (b) Zonally integrated and time-averaged meridional transport profile in the Atlantic at 26.5°N. The y-axis shows the depth (in km), and the x-axis shows the overturning (in Sv). (c) Scatter plot showing the overturning (in Sv) and the colored depth values (in km) for the meridional transport at 26.5°N.

**Figure 5** displays the zonally averaged distribution of vertically integrated global meridional heat transport. Positive (negative) values indicate transport northward (southward). The heat transport behaves as expected, transferring heat poleward in both hemispheres, consistent with the findings<sup>[59]</sup>. In the piControl simulation, the heat transport peaks at ~1.54 PW near 20°N in the Northern Hemisphere and ~1.16 PW near 11°S in the Southern Hemisphere. This difference in value and position is related to the South Atlantic Ocean advecting heat northward rather than poleward<sup>[60,61]</sup>.

Moreover, the maximum value of 1.54 PW near 20°N agrees with the 1.30 PW reached by the AMOC upper limb around 24.5°N<sup>[62]</sup>. This similarity reinforces the significant influence of the AMOC on global meridional heat transport. In the L-1pctCO<sub>2</sub> simulation, the northward heat transport decreases by 0.50 PW or 32.61%. This decrease is linked to a weakening

(38.64%) of the upper branch of the AMOC cell and its ability to advect heat northward. Conversely, the southward heat transport increases, which may be related to the strengthening of the lower AMOC cell.

### 3.2 The mixed layer depth

March is typically the month when the mixed layer of the North Atlantic is deepest<sup>[48,63,64]</sup> and is widely used in the literature as a benchmark for mixed layer depth analysis<sup>[63,65,66]</sup>. The evaluation of the mixed layer depth anomaly in March in the North Atlantic Ocean (not shown) revealed signals of mixed layer shallowing in crucial regions for the NADW formation<sup>[67,68]</sup> and hence the AMOC, mainly around the Labrador and Norwegian Seas, as well as southeast of Greenland. We have isolated the areas of mixed layer negative anomalies (red polygons in **Figure 1**) to better monitor them.

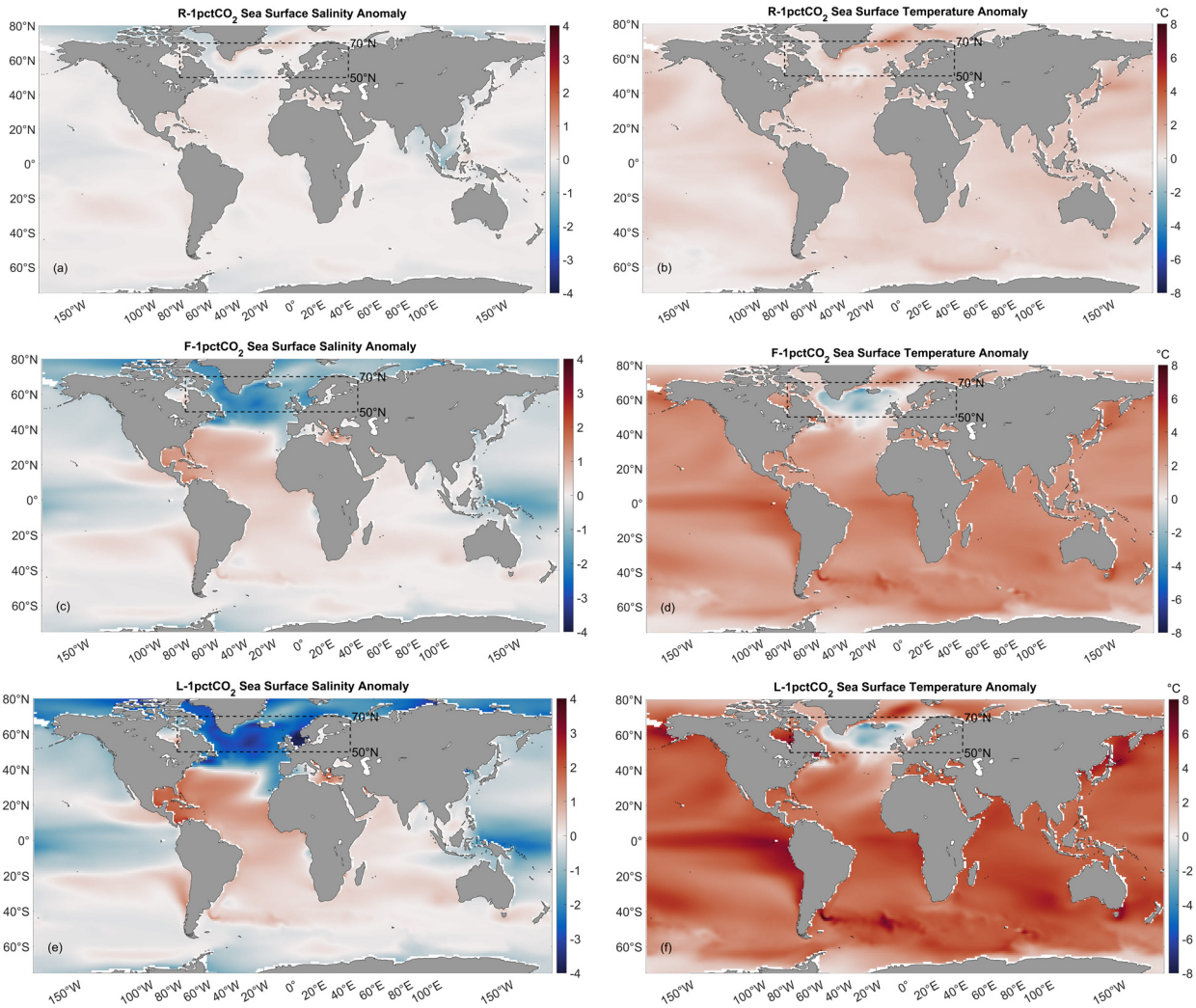


**Figure 4.** Anomalies of sea surface salinity (left panels) and sea surface temperature (right panels) in 1pctCO<sub>2</sub>, compared to the time average of 500 years of piControl. The top panels show the anomalies for R-1pctCO<sub>2</sub>, the middle panels show the anomalies for F-1pctCO<sub>2</sub>, and the lower panels show the anomalies for L-1pctCO<sub>2</sub>. Positive (negative) values indicate an increase (decrease) in the term relative to the average period of piControl. Additionally, the dashed region marks the area used to assess the freshwater flux between 50°N and 70°N.

The maximum mixed layer depth time series in March for each Area is shown in **Figure 6**. The piControl results indicate that all four Areas are relatively stable, and their values agree with those reported in previous studies<sup>[68,69]</sup>. However, in 1pctCO<sub>2</sub>, all areas experience a strong shallowing at different times. Area 1 shows the earliest and most pronounced shallowing, followed by the others<sup>[70]</sup>. Furthermore, the percentage reduction in mixed layer depth decreases from Area 1 to Areas 2, 3, and 4, indicating a cascade effect process. Specifically, the lag between consecutive areas is 25 years between Areas 1 and 2, 19 years between Areas 2 and 3, and 17 years between Areas

3 and 4, with corresponding lag-adjusted correlation values of 0.91, 0.89, and 0.86, respectively. This reduction in lag time between the areas is likely related to the amplification of global warming. Additionally, the variability in mixed layer depth practically reduces to zero (not shown), indicating that deep convection is shut down.

The reduction of mixed layer depth due to warming can increase the water column's stratification. Increased surface buoyancy leads to a more stratified water column<sup>[47]</sup>. To assess this effect in the simulations, we computed the surface buoyancy for Areas 1–4 using Equation (3). **Figure 7** shows each area's

time series of buoyancy. In the piControl simulation, we observe variability throughout the series with no discernible trend. However, in the 1pctCO<sub>2</sub> simulation, we observe a clear increase in buoyancy in the first few decades for all areas, particularly for Areas 1 and 2, which has direct implications for the formation of NADW. Area 3 exhibits oscillations and a smaller increase in buoyancy in the last decade compared to the other areas, which other factors beyond the scope of this study may influence.

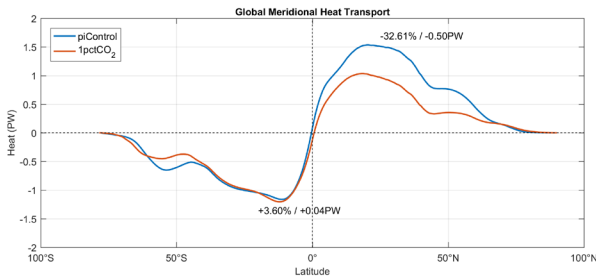


**Figure 5.** Latitudinal distribution of zonally averaged and depth-integrated heat transport (in petawatts, PW) for the time average of 500 years of piControl and L-1pctCO<sub>2</sub>. Furthermore, the texts show the percentage and absolute increase (+) or decrease (–) in L-1pctCO<sub>2</sub> compared to the average of piControl. The black dashed lines mark zero transport and 0° latitude.

### 3.3 Freshwater input to the North Atlantic Ocean

**Figure 8a** shows the time-averaged distribution of the total surface freshwater flux to the North Atlantic in piControl, expressed in mSv. The results are consistent with previous studies [71,72]. Although some regions have negative freshwater flux, particularly near Ireland, most of the North Atlantic experiences a net gain of freshwater, which reduces surface salinity and the buoyancy of the water. The freshwater input is overall low (ranging from 0 to 0.1 mSv), with higher values concentrated around the east coast of North America, the coast of Europe, and the west and east sides of Greenland, reaching up to 0.44 mSv, 0.33 mSv, 0.15 mSv, and 0.46 mSv, respectively.

The pattern of freshwater anomalies consistently intensifies from present to future, with the most significant changes occurring in the last decade. Specifically, there is a noticeable decrease in freshwater on

both sides of Greenland, in the north and northeast of Iceland and the eastern coast of North America, while the freshwater flux in the ocean interior increases. These changes could trigger modifications to the NADW formation, such as the weakening identified in this article and shown previously.

The average freshwater anomaly in L-1pctCO<sub>2</sub> (not shown) is  $7.00 \cdot 10^{-3}$  mSv, lower than the amounts reported in previous studies [12,13,17,18]. However, even this amount of freshwater input can cause significant changes in the AMOC cell, as seen previously [73]. Overall, these findings highlight the critical role of freshwater input in the ocean’s circulation and emphasize the potential impacts of even relatively small changes in this input.

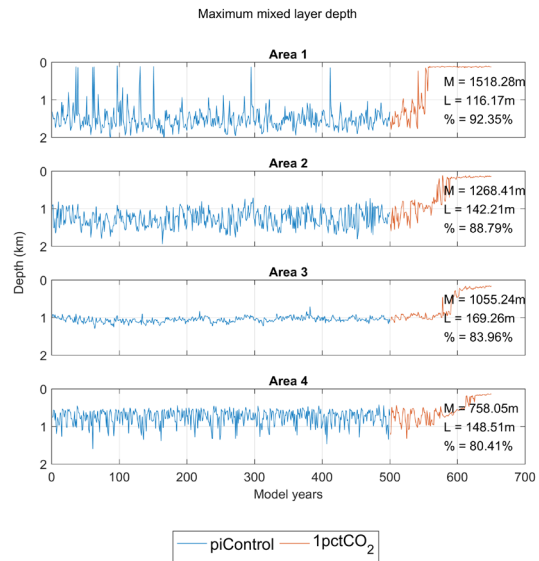


**Figure 6.** Time series of maximum mixed layer depth in March for each area (red polygons in **Figure 1**) in the piControl and 1pctCO<sub>2</sub> experiments. *M* represents the average piControl value, *L* is the average L-1pctCO<sub>2</sub> value, and % indicates the percentage of shallowing (decrease in mixed layer depth) in L-1pctCO<sub>2</sub> compared to the time average of 500 years of piControl. Shallowing refers to a reduction in the maximum depth of the mixed layer, which measures the depth of the layer in which temperature and salinity are relatively uniform.

**Figure 9** illustrates the behavior of each term used to estimate freshwater flux over time. The salt flux is not included as it is directly correlated with the sea ice melting flux, which showed a reduction of 92.64% in L-1pctCO<sub>2</sub>. Both sea ice terms exhibited reductions of over 85%, but their weak correlation

(0.55) indicates that different factors affect them. Meanwhile, the runoff flux increased throughout the experiment while the evaporation flux decreased. The precipitation flux exhibited fluctuations throughout the 150-year experiment, but the average value of L-1pctCO<sub>2</sub> was similar to the piControl mean.

It's worth noting that the variables related to sea ice showed high reductions, which is problematic because it is crucial for climate [74]. Diminished sea ice cover increases the surface area for atmospheric-ocean interaction and decreases the region's albedo, causing the ocean to absorb more heat, which leads to further melting. Reduced sea ice also increases the ocean's freshwater, which increases its buoyancy. Overall, these findings emphasize the importance of sea ice in regulating the Earth's climate and highlight the potential impacts of its reduction.

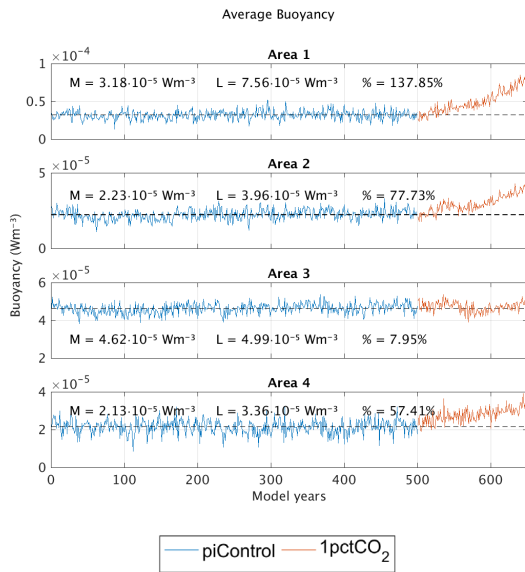


**Figure 7.** Buoyancy time series for each area (red polygons in **Figure 1**) in the piControl and 1pctCO<sub>2</sub> experiments. Buoyancy, a measure of the vertical stratification of the ocean, plays an important role in regulating ocean circulation and climate dynamics. The buoyancy was calculated using Equation (3).  $M$  represents the average piControl value,  $L$  is the L-1pctCO<sub>2</sub>, and % indicates the percentage of increase in L-1pctCO<sub>2</sub> compared to the time average of 500 years of piControl.

The amount of freshwater flux into the ocean is affected by several factors, including sea ice melting, evaporation, runoff, and frazil ice formation. Changes in each term can either increase or decrease

the freshwater flux, and the overall effect is complex and challenging to predict [57]. Our study found that the main factor driving changes in freshwater flux in L-1pctCO<sub>2</sub> was a decrease in evaporation flux, likely caused by colder SSTs in the North Atlantic. We observed that the evaporation flux and sea ice melting flux were strongly correlated, even though they had opposite effects on freshwater flux. This behavior suggests that climate stability may partly be due to the complex interplay between different factors affecting the ocean system.

A complex interplay of various factors determines the outcome of freshwater flux. We employed a decision tree algorithm to simulate the freshwater flux based on these factors, summarized in **Table 2**. The algorithm successfully obtained the freshwater flux with low RMSE and high R<sup>2</sup>, with runoff being the most critical predictor across all scenarios. Evaporation was the second most important predictor for R-, F-, and L-1pctCO<sub>2</sub>, followed by sea ice melting flux. For R- and L-1pctCO<sub>2</sub>, precipitation, and frazil fluxes were also significant predictors, while for F-1pctCO<sub>2</sub>, frazil and precipitation fluxes were significant.

In the past, we observed that runoff was the most critical factor limiting the total freshwater flux in the region. However, in the current climate, while the increasing tendency of runoff (**Figure 9**) still gives it a high score, it shares the importance with the evaporation flux, which is decreasing. This behavior is intensified on the L-1pctCO<sub>2</sub> with additional participation from the sea ice melting flux, which decreases drastically and justifies the higher score. At the end of 1pctCO<sub>2</sub>, the hydric balance (E-P) becomes more important. With colder SST (**Figure 4f**), the evaporation flux decreases, creating more high-pressure air masses, increasing surface pressure, and inhibiting the convection process.

It is crucial to notice that MOSART, the river transport model used at CESM2, only simulates the runoff process to the river and, consequently, the sea. It does not simulate the processes of infiltration, percolation, water storage in the saturated region of the ground (aquifer), and, subsequently, the discharge

of the aquifer into the sea. In this way, the process of transporting freshwater to the sea from the melting may be underestimated in the vast majority of Earth System Models, which use the same or similar models for this process, which would indicate that a possible collapse of the AMOC could happen much earlier than is being predicted.

Overall, our findings suggest that the amount of freshwater flux into the ocean is affected by a complex interplay of factors and that small changes in one term can significantly affect the overall system. By understanding these relationships, we can gain insights into the stability of the climate system and improve our ability to predict future changes.

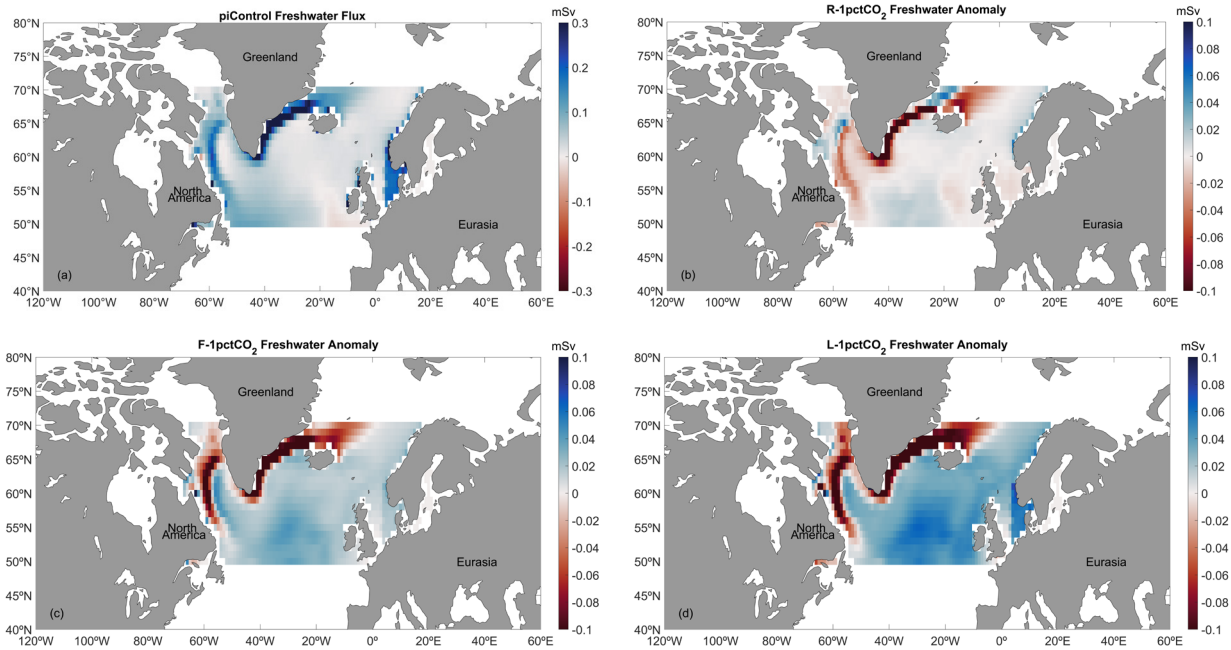


**Figure 8.** Freshwater flux to the North Atlantic Ocean, between 50°N and 70°N (the green region in **Figure 1**). (a) The time average of 500 years of piControl. (b) (c) and (d) represent R-1pctCO<sub>2</sub>, F-1pctCO<sub>2</sub>, and L-1pctCO<sub>2</sub> anomalies, respectively, compared to the time average of piControl. The color scale represents the freshwater flux anomaly (in miliSverdrups), and positive (negative) values indicate more (less) freshwater flux in 1pctCO<sub>2</sub> compared to piControl.

**Table 2.** The decision tree regressor is used to evaluate the most important components in the freshwater flux in monthly frequency. The top part of the table depicts statistical quantities (RMSE, R<sup>2</sup>) of the ability of the algorithm to represent the freshwater flux (dependent variable). The bottom part of the table depicts the scores of the variables used to calculate the freshwater flux (independent variables) for the 500y of piControl, the 150y of 1pctCO<sub>2</sub>, the 9y of R-1pctCO<sub>2</sub>, the 110y of the F-1pctCO<sub>2</sub> and the 10y of L-1pctCO<sub>2</sub>.

Metrics	piControl	1pctCO <sub>2</sub>	R-1pctCO <sub>2</sub>	F-1pctCO <sub>2</sub>	L-1pctCO <sub>2</sub>
RMSE (m <sup>3</sup> s <sup>-1</sup> )	0.050	0.073	0.028	0.071	0.040
R <sup>2</sup>	0.913	0.822	0.979	0.979	0.907
Scores	piControl	1pctCO <sub>2</sub>	R-1pctCO <sub>2</sub>	F-1pctCO <sub>2</sub>	L-1pctCO <sub>2</sub>
Sea ice melting flux	0.105	0.076	0.086	0.071	0.167
Frazil flux	0.001	0.041	0.017	0.070	0.022
Runoff flux	0.886	0.811	0.739	0.753	0.559
Precipitation flux	0.003	0.021	0.023	0.020	0.045
Evaporation flux	0.005	0.051	0.136	0.085	0.207

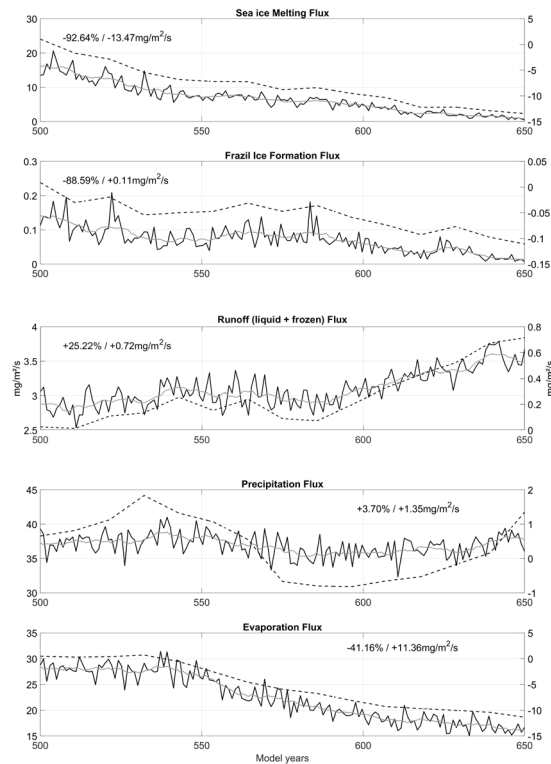


**Figure 9.** Annual mean series of terms used to calculate the 1pctCO<sub>2</sub> experiment freshwater (in mg/m<sup>2</sup>/s). The left y-axis corresponds to the continuous black and gray lines, which show the flux and the 10-year moving average from each series, respectively. The right y-axis corresponds to the dashed black lines showing decadal anomalies. The green region in **Figure 1** represents the area considered for the calculation.

## 4. Conclusions

This study focused on the impacts of increased atmospheric CO<sub>2</sub> on the AMOC dynamics and related mechanisms between the ocean, sea ice, and atmosphere using Earth System model results with CO<sub>2</sub> forcing. The significant decrease in the time series of the overturning was due to the weakening and shallowing of the AMOC upper branch and the strengthening and stretching of the lower branch, which confined the upper branch to shallower waters.

The freshening in high latitudes of the North Atlantic led to a shallower mixed layer depth and reduced deep convection, resulting in a decrease in NADW formation and an increase in AABW formation and spread. These changes, in turn, weakened the upper branch of the AMOC, resulting in less heat

reaching high latitudes in the North Atlantic, which was evident from the warming hole observed on the surface of the North Atlantic Ocean.

This work noted that the observed data showed that the AMOC weakening conditions were more pronounced than in the CESM2 simulations (R-1pctCO<sub>2</sub>). This behavior may be associated with simulating the complex heat, mass, and momentum fluxes in the ocean-atmosphere and soil-ice-atmosphere interactions.

During the last decade of the experiment (L-1pctCO<sub>2</sub>), there was a significant drop in ocean evaporation and sea ice and an increase in river runoff. The lower SSTs in the warming hole area, caused by melted sea ice, resulted in reduced evaporation and surface salinity. At the same time, the increase in runoff led to more freshwater being sent to the ocean, creating a positive feedback loop. The model seems to underestimate the impact of this positive feedback loop, as observed in the current climate (RAPID vs. R-1pctCO<sub>2</sub>). This underestimation could potentially lead to a faster disruption of the AMOC than what is being predicted by Earth System models.

While we have not yet reached a moment of a pattern change in the climate system, the increasing intensity and frequency of extreme events indicate the amplification of climate variability due to additional energy being added to the system. The probability of this process accelerating is closely linked to our socioeconomic model of unrestrained consumption, unclean energy production, and planned obsolescence. Future research could explore potential impacts on other aspects of the world's ocean and atmosphere, building on the findings presented here.

## Author Contributions

All authors contributed to the conceptualization of the study. Lívia Sancho, Luiz Paulo Assad, and Luiz Landau were responsible for the resources. Lívia Sancho and Elisa Passos were responsible for the software, formal analysis, and manuscript writing. Lívia Sancho, Elisa Passos, Luiz Paulo de Freitas Assad, and Marcio Cataldi conceived and reviewed the manuscript. Luiz Paulo de Freitas Assad, Marcio Cataldi, and Luiz Landau edited the text.

Luiz Paulo Assad and Luiz Landau were responsible for the funding acquisition. All authors read and approved the final manuscript.

## Conflict of Interest

The authors declare that the research was conducted without any commercial or financial relationship that could be construed as a potential conflict of interest.

## Data Availability

CMIP6 outputs are available from the following websites: <https://esgfnode.llnl.gov/search/cmip6/>, <https://esgf-node.ipsl.upmc.fr/search/cmip6-ipsl/>, <https://esgf-node.ipsl.upmc.fr/search/cmip6-ipsl/> and <https://esgfindex1.ceda.ac.uk/search/cmip6-ceda/>.

The Natural Environment Research Council funds data from the RAPID AMOC monitoring project (<https://doi.org/10.5285/e91b10af-6f0a-7fa7-e053-6c86abc05a09>) and are freely available from [www.rapid.ac.uk/rapidmoc](http://www.rapid.ac.uk/rapidmoc).

Mauna Loa CO<sub>2</sub> records (<https://doi.org/10.6075/J0QJ7F7N>) are also freely available from <https://library.ucsd.edu/dc/object/bb90132731>.

## Funding

This work was possible through the financing of PEC-20480 Project between Royal Dutch Shell (Shell) and the *Laboratório de Métodos Computacionais em Engenharia* (LAMCE) and through the doctoral fellowship funding by CNPq for Elisa Passos Case number 141819/2016-2 and the postdoctoral fellowship funding by FAPERJ E 10/2020—*Edital Inteligência Artificial* Case Number E-26/203.327/2022—Enrollment No. Scholarship 2015.08297.7 for Livia Sancho.

## Acknowledgments

We gratefully acknowledge the *Universidade Federal do Rio de Janeiro* (UFRJ), the *Instituto Alberto Luiz Coimbra de Pós-Graduação e Pesquisa de Engenharia* (COPPE), the *Programa de Engenharia Civil*, the *Conselho Nacional de Desenvolvimento*

*Científico e Tecnológico* (CNPq) and the *Fundação de Amparo à Pesquisa do Estado do Rio de Janeiro* (FAPERJ) for granting the opportunity to develop this work.

## References

- [1] Global Warming of 1.5 °C [Internet]. IPCC. Available from: [https://www.ipcc.ch/site/assets/uploads/sites/2/2019/06/SR15\\_Full\\_Report\\_High\\_Res.pdf](https://www.ipcc.ch/site/assets/uploads/sites/2/2019/06/SR15_Full_Report_High_Res.pdf)
- [2] Costello, A., Abbas, M., Allen, A., et al., 2009. Managing the health effects of climate change: lancet and University College London Institute for Global Health Commission. *The Lancet*. 373(9676), 1693–1733. DOI: [https://doi.org/10.1016/S0140-6736\(09\)60935-1](https://doi.org/10.1016/S0140-6736(09)60935-1)
- [3] IPCC, 2013. Summary for policymakers. Cambridge University Press: Cambridge. DOI: <https://doi.org/10.1017/CBO9781107415324.004>
- [4] Sundquist, E.T., 2013. Geological perspectives on carbon dioxide and the carbon cycle. American Geophysical Union (AGU): Washington, D.C. pp. 5–60. DOI: <https://doi.org/10.1029/GM032p0005>
- [5] Broecker, W.S., 1987. Unpleasant surprises in the greenhouse? *Nature*. 328, 123–126. DOI: <https://doi.org/10.1038/328123a0>
- [6] Broecker, W.S., 1997. Thermohaline circulation, the Achilles heel of our climate system: Will man-made CO<sub>2</sub> upset the current balance? *Science*. 278(5343), 1582–1588. DOI: <https://doi.org/10.1126/science.278.5343.1582>
- [7] Jackson, L.C., Biastoch, A., Buckley, M.W., et al., 2022. The evolution of the North Atlantic meridional overturning circulation since 1980. *Nature Reviews Earth & Environment*. 3, 241–254. DOI: <https://doi.org/10.1038/s43017-022-00263-2>
- [8] Johnson, H.L., Cessi, P., Marshall, D.P., et al., 2019. Recent contributions of theory to our understanding of the Atlantic meridional overturning circulation. *Journal of Geophysical Research*

- search: *Oceans*. 124(8), 5376–5399.  
DOI: <https://doi.org/10.1029/2019JC015330>
- [9] Frajka-Williams, E., Foukal, N., Danabasoglu, G., 2023. Should AMOC observations continue: How and why?. *Philosophical Transactions of the Royal Society A*. 381(2262).  
DOI: <https://doi.org/10.1098/rsta.2022.0195>
- [10] Anthonoff, D., Estrada, F., Tol, R.S., 2016. Shutting down the thermohaline circulation. *American Economic Review*. 106(5), 602–606.  
DOI: <https://doi.org/10.1257/aer.p20161102>
- [11] Danabasoglu, G., Yeager, S.G., Kim, W.M., et al., 2016. North Atlantic simulations in Coordinated Ocean-ice Reference Experiments phase II (CORE-II). Part II: Inter-annual to decadal variability. *Ocean Modelling*. 97, 65–90.  
DOI: <https://doi.org/https://doi.org/10.1016/j.ocemod.2015.11.007>
- [12] Stocker, T.F., Wright, D.G., 1991. Rapid transitions of the ocean's deep circulation induced by changes in surface water fluxes. *Nature*. 351, 729–732.  
DOI: <https://doi.org/10.1038/351729a0>
- [13] Lenton, T.M., Held, H., Kriegler, E., et al., 2008. Tipping elements in the Earth's climate system. *Proceedings of the national Academy of Sciences*. 105(6), 1786–1793.  
DOI: <https://doi.org/10.1073/pnas.0705414105>
- [14] Orihuela-Pinto, B., England, M.H., Taschetto, A.S., 2022. Interbasin and interhemispheric impacts of a collapsed Atlantic Overturning Circulation. *Nature Climate Change*. 12, 558–565.  
DOI: <https://doi.org/10.1038/s41558-022-01380-y>
- [15] Luo, Y., Tjiputra, J., Guo, C., et al., 2018. Atlantic deep water circulation during the last interglacial. *Scientific Reports*. 8, 4401.  
DOI: <https://doi.org/10.1038/s41598-018-22534-z>
- [16] Buckley, M.W., Marshall, J., 2016. Observations, inferences, and mechanisms of the Atlantic Meridional Overturning Circulation: A review. *Reviews of Geophysics*. 54(1), 5–63.  
DOI: <https://doi.org/10.1002/2015RG000493>
- [17] Manabe, S., Stouffer, R.J., 1999. The role of thermohaline circulation in climate. *Tellus A: Dynamic Meteorology and Oceanography*. 51(1), 91–109.
- [18] Vellinga, M., Wood, R.A., 2002. Global climatic impacts of a collapse of the Atlantic thermohaline circulation. *Climatic Change*. 54, 251–267.  
DOI: <https://doi.org/10.1023/A:1016168827653>
- [19] Knutti, R., Masson, D., Gettelman, A., 2013. Climate model genealogy: Generation CMIP5 and how we got there. *Geophysical Research Letters*. 40(6), 1194–1199.  
DOI: <https://doi.org/10.1002/grl.50256>
- [20] Danabasoglu, G., Lamarque, J.F., Bacmeister, J., et al., 2020. The community earth system model version 2 (CESM2). *Journal of Advances in Modeling Earth Systems*. 12(2), e2019MS001916.  
DOI: <https://doi.org/10.1029/2019MS001916>
- [21] Cam6.3 User's Guide [Internet]. NCAR: National Center for Atmospheric Research [cited 2023 Dec 23]. Available from: <https://doi.org/10.5065/Z953-ZC95>
- [22] Lawrence, D.M., Fisher, R.A., Koven, C.D., et al., 2019. The Community Land Model version 5: Description of new features, benchmarking, and impact of forcing uncertainty. *Journal of Advances in Modeling Earth Systems*. 11(12), 4245–4287.  
DOI: <https://doi.org/10.1029/2018MS001583>
- [23] Technical Description of Version 4.0 of the Community Land Model (CLM) [Internet]. NCAR: National Center for Atmospheric Research. Available from: <https://opensky.ucar.edu/islandora/object/technotes%3A493/datastream/PDF/view>
- [24] Hurrell, J.W., Holland, M.M., Gent, P.R., et al., 2013. The community earth system model: A framework for collaborative research. *Bulletin of the American Meteorological Society*. 94(9), 1339–1360.  
DOI: <https://doi.org/10.1175/BAMS-D-12-00121.1>
- [25] CICE: The Los Alamos Sea Ice Model Docu-

- mentation and Software User's Manual Version 4.1 LA-CC-06-012 [Internet]. Los Alamos National Laboratory. Available from: [https://csdms.colorado.edu/w/images/CICE\\_documentation\\_and\\_software\\_user%27s\\_manual.pdf](https://csdms.colorado.edu/w/images/CICE_documentation_and_software_user%27s_manual.pdf)
- [26] Hunke, E.C., Dukowicz, J.K., 2002. The elastic-viscous-plastic sea ice dynamics model in general orthogonal curvilinear coordinates on a sphere—Incorporation of metric terms. *Monthly Weather Review*. 130(7), 1848–1865. DOI: [https://doi.org/10.1175/1520-0493\(2002\)130<1848:TEVPSI>2.0.CO;2](https://doi.org/10.1175/1520-0493(2002)130<1848:TEVPSI>2.0.CO;2)
- [27] Bitz, C.M., Lipscomb, W.H., 1999. An energy-conserving thermodynamic model of sea ice. *Journal of Geophysical Research: Oceans*. 104(C7), 15669–15677. DOI: <https://doi.org/10.1029/1999JC900100>
- [28] A Delta-Eddington Multiple Scattering Parameterization for Solar Radiation in the Sea Ice Component of the Community Climate System Model (No. NCAR/TN-472+STR) [Internet]. [cited 2023 Dec 23]. Available from: <https://doi.org/10.5065/D6B27S71>
- [29] Holland, M.M., Bailey, D.A., Briegleb, B.P., et al., 2012. Improved sea ice shortwave radiation physics in CCSM4: The impact of melt ponds and aerosols on Arctic sea ice. *Journal of Climate*. 25(5), 1413–1430. DOI: <https://doi.org/10.1175/JCLI-D-11-00078.1>
- [30] Thorndike, A.S., Rothrock, D.A., Maykut, G.A., et al., 1975. The thickness distribution of sea ice. *Journal of Geophysical Research*. 80(33), 4501–4513. DOI: <https://doi.org/10.1029/JC080i033p04501>
- [31] Li, H., Wigmosta, M.S., Wu, H., et al., 2013. A physically based runoff routing model for land surface and earth system models. *Journal of Hydrometeorology*. 14(3), 808–828. DOI: <https://doi.org/10.1175/JHM-D-12-015.1>
- [32] The Parallel Ocean Program (POP) Reference Manual: Ocean Component of the Community Climate System Model (CCSM) and Community Earth System Model (CESM) [Internet]. Los Alamos National Laboratory. Available from: <https://opensky.ucar.edu/islandora/object/manuscripts%3A825/datastream/PDF/view>
- [33] Griffies, S.M., Böning, C., Bryan, F.O., et al., 2000. Developments in ocean climate modeling. *Ocean Modelling*. 2(3–4), 123–192. DOI: [https://doi.org/10.1016/S1463-5003\(00\)00014-7](https://doi.org/10.1016/S1463-5003(00)00014-7)
- [34] Eyring, V., Bony, S., Meehl, G.A., et al., 2016. Overview of the Coupled Model Intercomparison Project Phase 6 (CMIP6) experimental design and organization. *Geoscientific Model Development*. 9(5), 1937–1958. DOI: <https://doi.org/10.5194/gmd-9-1937-2016>
- [35] Meinshausen, M., Vogel, E., Nauels, A., et al., 2017. Historical greenhouse gas concentrations for climate modelling (CMIP6). *Geoscientific Model Development*. 10(5), 2057–2116. DOI: <https://doi.org/10.5194/gmd-10-2057-2017>
- [36] Hoesly, R.M., Smith, S.J., Feng, L., et al., 2018. Historical (1750–2014) anthropogenic emissions of reactive gases and aerosols from the Community Emissions Data System (CEDS). *Geoscientific Model Development*. 11(1), 369–408. DOI: <https://doi.org/10.5194/gmd-11-369-2018>
- [37] Van Marle, M.J., Kloster, S., Magi, B.I., et al., 2017. Historic global biomass burning emissions for CMIP6 (BB4CMIP) based on merging satellite observations with proxies and fire models (1750–2015). *Geoscientific Model Development*. 10(9), 3329–3357. DOI: <https://doi.org/10.5194/gmd-10-3329-2017>
- [38] Kay, J.E., Deser, C., Phillips, A., et al., 2015. The Community Earth System Model (CESM) large ensemble project: A community resource for studying climate change in the presence of internal climate variability. *Bulletin of the American Meteorological Society*. 96(8), 1333–1349. DOI: <https://doi.org/10.1175/BAMS-D-13-00255.1>

- [39] Steele, M., Morley, R., Ermold, W., 2001. PHC: A global ocean hydrography with a high-quality Arctic Ocean. *Journal of Climate*. 14(9), 2079–2087.  
DOI: [https://doi.org/10.1175/1520-0442\(2001\)014<2079:PAGOHW>2.0.CO;2](https://doi.org/10.1175/1520-0442(2001)014<2079:PAGOHW>2.0.CO;2)
- [40] Bacmeister, J.T., Hannay, C., Medeiros, B., et al., 2020. CO<sub>2</sub> increase experiments using the CESM: Relationship to climate sensitivity and comparison of CESM1 to CESM2. *ESS Open Archive*.  
DOI: <https://doi.org/10.1002/essoar.10502611.1>
- [41] Atlantic Meridional Overturning Circulation Observed by the RAPID-MOCHA-WBTS (Rapid-Meridional Overturning Circulation and Heatflux Array-Western Boundary Time Series) Array at 26N from 2004 to 2022 (v2022.1) [Internet]. British Oceanographic Data Centre. [cited 2023 Nov 11]. Available from: <https://doi.org/10.5285/04c79ece-3186-349a-e063-6c86abc0158c>
- [42] Lozier, M.S., Bacon, S., Bower, A.S., et al., 2017. Overturning in the Subpolar North Atlantic Program: A new international ocean observing system. *Bulletin of the American Meteorological Society*. 98(4), 737–752.  
DOI: <https://doi.org/10.1175/BAMS-D-16-0057.1>
- [43] McCarthy, G.D., Smeed, D.A., Johns, W.E., et al., 2015. Measuring the Atlantic meridional overturning circulation at 26°N. *Progress in Oceanography*. 130, 91–111.  
DOI: <https://doi.org/10.1016/j.pocean.2014.10.006>
- [44] Frajka-Williams, E., Ansorge, I.J., Baehr, J., et al., 2019. Atlantic meridional overturning circulation: Observed transport and variability. *Frontiers in Marine Science*. 6, 260.  
DOI: <https://doi.org/10.3389/fmars.2019.00260>
- [45] Kim, S.K., Kim, H.J., Dijkstra, H.A., et al., 2022. Slow and soft passage through tipping point of the Atlantic Meridional Overturning Circulation in a changing climate. *npj Climate and Atmospheric Science*. 5, 13.  
DOI: <https://doi.org/10.1038/s41612-022-00236-8>
- [46] Manabe, S., Stouffer, R.J., 1997. Coupled ocean-atmosphere model response to freshwater input: Comparison to Younger Dryas event. *Paleoceanography and Paleoclimatology*. 12(2), 321–336.  
DOI: <https://doi.org/10.1029/96PA03932>
- [47] Castro, B.M., 2014. Summer/winter stratification variability in the central part of the South Brazil Bight. *Continental Shelf Research*. 89, 15–23.  
DOI: <https://doi.org/10.1016/j.csr.2013.12.002>
- [48] Large, W.G., Danabasoglu, G., Doney, S.C., et al., 1997. Sensitivity to surface forcing and boundary layer mixing in a global ocean model: Annual-mean climatology. *Journal of Physical Oceanography*. 27(11), 2418–2447.  
DOI: [https://doi.org/10.1175/1520-0485\(1997\)027<2418:STSFAB>2.0.CO;2](https://doi.org/10.1175/1520-0485(1997)027<2418:STSFAB>2.0.CO;2)
- [49] Kadiyala, A., Kumar, A., 2017. Applications of Python to evaluate environmental data science problems. *Environmental Progress & Sustainable Energy*. 36(6), 1580–1586.  
DOI: <https://doi.org/10.1002/ep.12786>
- [50] Loh, W.Y., 2011. Classification and regression trees. *Wiley Interdisciplinary Reviews: Data Mining and Knowledge Discovery*. 1(1), 14–23.  
DOI: <https://doi.org/10.1002/widm.8>
- [51] Pedregosa, F., Varoquaux, G., Gramfort, A., et al., 2011. Scikit-learn: Machine learning in Python. *The Journal of Machine Learning Research*. 12, 2825–2830.  
DOI: <https://doi.org/10.1002/widm.8>
- [52] De'ath, G., Fabricius, K.E., 2000. Classification and regression trees: A powerful yet simple technique for ecological data analysis. *Ecology*. 81(11), 3178–3192.  
DOI: [https://doi.org/10.1890/0012-9658\(2000\)081\[3178:CARTAP\]2.0.CO;2](https://doi.org/10.1890/0012-9658(2000)081[3178:CARTAP]2.0.CO;2)
- [53] Moat, B.I., Smeed, D.A., Frajka-Williams, E., et al., 2020. Pending recovery in the strength of the meridional overturning circulation at 26°N. *Ocean Science*. 16(4), 863–874.  
DOI: <https://doi.org/10.5194/os-16-863-2020>
- [54] Smeed, D.A., Josey, S.A., Beaulieu, C., et al.,

2018. The North Atlantic Ocean is in a state of reduced overturning. *Geophysical Research Letters*. 45(3), 1527–1533.  
DOI: <https://doi.org/10.1002/2017GL076350>
- [55] Atlantic Meridional Overturning Circulation Observed by the RAPID-MOCHA-WBTS (RAPID-Meridional Overturning Circulation and Heatflux Array-Western Boundary Time Series) Array at 26N from 2004 to 2020 (v2020.1) [Internet]. National Oceanography Centre. Available from: <https://doi.org/10.5285/cc1e34b3-3385-662b-e053-6c86abc03444>
- [56] Jackson, L.C., Hewitt, H.T., Bruciaferri, D., et al., 2023. Challenges simulating the AMOC in climate models. *Philosophical Transactions of the Royal Society A*. 381(2262), 20220187.  
DOI: <https://doi.org/10.1098/Rsta.2022.0187>
- [57] Swingedouw, D., Mignot, J., Braconnot, P., et al., 2009. Impact of freshwater release in the North Atlantic under different climate conditions in an OAGCM. *Journal of Climate*. 22(23), 6377–6403.  
DOI: <https://doi.org/10.1175/2009JCLI3028.1>
- [58] Boers, N., 2021. Observation-based early-warning signals for a collapse of the Atlantic Meridional Overturning Circulation. *Nature Climate Change*. 11(8), 680–688.  
DOI: <https://doi.org/10.1038/s41558-021-01097-4>
- [59] Stammer, D., Köhl, A., Vlasenko, A., et al., 2018. A pilot climate sensitivity study using the CEN coupled adjoint model (CESAM). *Journal of Climate*. 31(5), 2031–2056.  
DOI: <https://doi.org/10.1175/JCLI-D-17-0183.1>
- [60] Sancho, L.M.B., de Freitas Assad, L.P., Landau, L., 2015. Volume and heat transports analysis in the South Atlantic Basin related to climate change scenarios. *Brazilian Journal of Geophysics*. 33(2), 333–348.  
DOI: <http://dx.doi.org/10.22564/rbgf.v33i2.724>
- [61] Zhu, Y., Wei, Z., Wang, Y., et al., 2014. The annual mean sketches and climatological variability of the volume and heat transports through the inter-basin passages: A study based on 1400-year spin up of MOM4p1. *Acta Oceanologica Sinica*. 33, 12–24.  
DOI: <https://doi.org/10.1007/s13131-014-0513-7>
- [62] Srokosz, M., Baringer, M., Bryden, H., et al., 2012. Past, present, and future changes in the Atlantic meridional overturning circulation. *Bulletin of the American Meteorological Society*. 93(11), 1663–1676.  
DOI: <https://doi.org/10.1175/BAMS-D-11-00151.1>
- [63] Lique, C., Johnson, H.L., Plancherel, Y., 2018. Emergence of deep convection in the Arctic Ocean under a warming climate. *Climate Dynamics*. 50, 3833–3847.  
DOI: <https://doi.org/10.1007/s00382-017-3849-9>
- [64] Carton, J.A., Grodsky, S.A., Liu, H., 2008. Variability of the oceanic mixed layer, 1960–2004. *Journal of Climate*. 21(5), 1029–1047.  
DOI: <https://doi.org/10.1175/2007JCLI1798.1>
- [65] Lohmann, K., Drange, H., Bentsen, M., 2009. Response of the North Atlantic subpolar gyre to persistent North Atlantic oscillation like forcing. *Climate Dynamics*. 32, 273–285.  
DOI: <https://doi.org/10.1007/s00382-008-0467-6>
- [66] Mauritzen, C., Häkkinen, S., 1997. Influence of sea ice on the thermohaline circulation in the Arctic-North Atlantic Ocean. *Geophysical Research Letters*. 24(24), 3257–3260.  
DOI: <https://doi.org/10.1029/97GL03192>
- [67] Colling, A., 1989. *Ocean circulation*. Elsevier: Oxford.
- [68] Talley, L., Pickard, G., Emery, W., et al., 2011. *Descriptive physical oceanography: An introduction*. Elsevier: Boston.
- [69] Grassl, H., 2001. *The ocean and climate: Climate and oceans. Ocean circulation and climate: Observing and modelling the global ocean*. Academic Press: Cambridge. pp. 3–10.
- [70] Muntjewerf, L., Sellevold, R., Vizcaino, M., et al., 2020. Accelerated Greenland ice sheet mass loss under high greenhouse gas forcing as simulated by the coupled CESM2. 1-CISM2. 1. *Journal of Advances in Modeling Earth Sys-*

- tems. 12(10), e2019MS002031.  
DOI: <https://doi.org/10.1029/2019MS002031>
- [71] Forryan, A., Bacon, S., Tsubouchi, T., et al., 2019. Arctic freshwater fluxes: Sources, tracer budgets and inconsistencies. *The Cryosphere*. 13(8), 2111–2131.  
DOI: <https://doi.org/10.5194/tc-13-2111-2019>
- [72] McDonagh, E.L., King, B.A., Bryden, H.L., et al., 2015. Continuous estimate of Atlantic oceanic freshwater flux at 26.5°N. *Journal of Climate*. 28(22), 8888–8906.  
DOI: <https://doi.org/10.1175/JCLI-D-14-00519.1>
- [73] Rahmstorf, S., 1995. Climate drift in an ocean model coupled to a simple, perfectly matched atmosphere. *Climate Dynamics*. 11, 447–458.  
DOI: <https://doi.org/10.1007/BF00207194>
- [74] Bitz, C.M., Holland, M.M., Hunke, E.C., et al., 2005. Maintenance of the sea-ice edge. *Journal of Climate*. 18(15), 2903–2921.  
DOI: <https://doi.org/10.1175/JCLI3428.1>